arXiv:1412.8675v1 [cond-mat.mtrl-sci] 30 Dec 2014

Emergence of ferroelectricity and spin-valley properties in two-dimensional honeycomb binary compounds.

Domenico Di Sante,[1,2] Alessandro Stroppa,[1] Paolo Barone,[1] Myung-Hwan Whangbo,[3] and Silvia Picozzi[1]

[1]*Consiglio Nazionale delle Ricerche (CNR-SPIN), Via Vetoio, L'Aquila, Italy*
[2]*Department of Physical and Chemical Sciences, University of L'Aquila, Via Vetoio 10, I-67010 L'Aquila, Italy**
[3]*Department of Chemistry, North Carolina State University, Raleigh, North Carolina 27695-8204, U.S.A.*

(Dated: December 31, 2014)

By means of density functional theory calculations, we predict that several two dimensional AB binary monolayers, where A and B atoms belong to group IV or III-V, are ferroelectric. Dipoles arise from the buckled structure, where the A and B ions are located on the sites of a bipartite corrugated honeycomb lattice with trigonal symmetry. We discuss the emerging valley-dependent properties and the coupling of spin and valley physics, which arise from the loss of inversion symmetry, and explore the interplay between ferroelectricity and Rashba spin-spitting phenomena. We show that valley-related properties originate mainly from the binary nature of AB monolayers, while the Rashba spin-texture developing around valleys is fully controllable and switchable by reversing the ferroelectric polarization.

INTRODUCTION

A wide range of modern electronic applications are based on the charge and spin degrees of freedom (DOF) of electrons. Two-dimensional (2D) atomic crystals with honeycomb lattice, such as graphene and molybdenum disulfide (MoS_2) monolayer, have recently been the object of intense research activities due to the additional valley DOF of carriers that might be useful in next-generation electronics applications [1–13]. In the 2D semimetal graphene [1–4], the π and π^* bands linearly cross at K and -K points of the hexagonal Brillouin zone (BZ), implying that charge carriers behave like massless Dirac fermions; at the same time, when spin-orbit coupling (SOC) is taken into account, the electrons experience opposite effective magnetic fields with equal magnitude at the K and -K valleys (related by time-reversal symmetry). In principle, valley DOFs in graphene could be exploited for valley-dependent electronics and opto-electronics, but their control by electrical and optical means is difficult due to the inversion symmetry of the graphene crystal structure, preventing the appearance of valley-contrasting properties[12, 14]. On the other hand, the 2D MoS_2 semiconductor [5–13] monolayer has no inversion symmetry and displays a direct band gap at the K and -K valleys, enabling optical pumping of valley-polarized carriers by shining the monolayer with circularly polarized light[5, 6]. In addition, when electrically biased, electrons from the K and -K valleys of MoS_2 monolayer experience opposite Lorentz-like forces giving rise to a valley Hall effect (VHE). To measure the VHE, it is necessary to irradiate the layer with circularly polarized photons (with the electric field applied parallel to the layer) so that electrons are excited only from valley K (or -K) thus breaking time-reversal symmetry[11, 12].

Using first-principle calculations, Ciraci *et al.* investigated two-dimensional honeycomb structures of group-IV elements and their binary compounds as well as the compounds of group III-V elements[15]. It was found that buckled AB monolayers with trigonal symmetry (*e.g.*, group IV binary monolayers SiGe, SiSn, GeSn and group III-V binary monolayers AlSb, GaP, GaAs, InP, InAs,

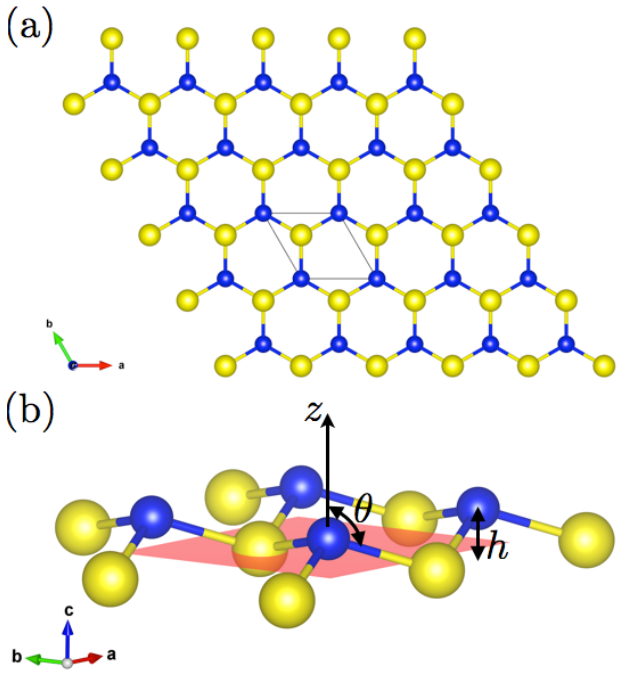

FIG. 1: (AB = SiGe, SiSn, GeSn, AlSb, GaP, GaAs, InP, InAs, InSb) (a) Top view of a buckled AB monolayer along the c-direction. (b) 3D view of a buckled AB monolayer, where the trigonal sheet of A is separated by a distance h from that of B. The buckling angle θ is defined as the angle between an A-B bond and the z direction normal to the plane. AB→BA conversion and the consequent ferroelectric switching occurs when θ crosses $\pi/2$.

TABLE I: Buckling angle θ (deg), buckling height h (Å), band gap E_g (eV), barrier height E_a (eV/fu), polarization P (10^{-12} C/m) and valence ΔE_{VB} and conduction ΔE_{CB} spin-splittings (meV) at the K point of buckled AB monolayers.

	θ (deg)	h (Å)	E_g (eV)	E_a (eV/fu)	P ($10^{-12} C/m$)	ΔE_{VB} (meV)	ΔE_{CB} (meV)
SiGe	105.1	0.60	0.02	0.16	0.88	25.3	5.8
SiSn	105.4	0.72	0.98	0.23	4.22	79.8	38.0
GeSn	108.2	0.81	0.21	0.39	3.22	70.0	19.1
AlSb	105.2	0.68	1.43	0.14	7.82	20.0	50.8
GaP	101.3	0.44	2.16	0.05	9.24	7.4	5.3
GaAs	105.3	0.63	1.74	0.18	9.07	14.9	33.8
InP	102.4	0.53	1.33	0.07	11.45	21.0	10.4
InAs	105.9	0.70	0.87	0.22	11.10	36.4	45.8
InSb	107.5	0.83	0.69	0.30	8.30	57.2	100.9

InSb) [15], in which a trigonal sublattice of A ions is separated from that of B ions (Fig. 1a), are more stable with respect to a planar geometry. The tendency to a buckled geometry was explained in terms of the destabilization of the π bonds in sp^2 hybridization due to the increase of the bond length between the two atoms A and B, as it happens in silicene and germanene compared to graphene.[16] As a result of the buckling, the sp^2 states dehybridize and the s,p_x,p_y orbitals combine with p_z orbitals to form new sp^3-like orbitals. Three of these sp^3 states form covalent bonds with three nearest-neighbor atoms, while one sp^3-like orbital directed upward perpendicular to the atomic plane forms a weak bond with the adjacent sp^3-like orbital directed downward. Interestingly, silicene and germanene are expected to display valley-contrasting properties analogous to graphene as soon as the inversion symmetry is broken, e.g., by applying an external electric field.[16] Therefore, other buckled honeycomb lattices are expected to display similar valley-dependent properties. Furthermore, in *buckled* trigonal structure, one can introduce a *sublattice pseudospin* ζ describing the binary layer DOF[12]: the pseudospin ζ up (down) refers to the state where the charge carrier is located in the upper (lower) layer, or equivalently in the A (B) sublattice. Therefore, a pseudospin polarization would directly correspond to an electrical polarization. In fact, buckled AB monolayers have no inversion symmetry and actually belong to the *polar* space group $P3m_1$, with the polar axis perpendicular to the layer (Fig. 1b), possibly leading to a ferroelectric (FE) state; in addition to the emergence of valley-contrasting physics, therefore, they can also display a Rashba effect[17], which would likely be coupled to and controllable with the FE polarization. If this is the case, it would be possible to act on the spin DOFs of these valley-active systems by reversing the FE polarization of the monolayer [18]. We explore this possibility in the present work, where we theoretically predict, by density functional calculations complemented with model Hamiltonian analysis, that the buckled group IV and group III-V binary monolayers with trigonal symmetry[15] are 2D ferroelectrics with spin-valley coupling and Rashba effects in their electronic structure. We show that SOC and a bipartite honeycomb lattice with different A and B atoms are at the origin of a spin-valley-sublattice coupling which is responsible for a valley-dependent Zeeman-like splitting at the K and -K valleys, while a nonvanishing buckling is responsible for an in-plane Rashba spin-texture that is controllable by electric field.

From the experimental point of view, several top-down and bottom-up methods have been proposed and devised for synthesizing 2D materials, as reported in recent review papers[19, 20]. Specifically, both silicene and germanene have been proven to exist as a monolayer when grown on selected metal substrates. Although bulk Si cannot form a layered phase like graphite, experiments of surface-assisted epitaxial growth show the presence of nanoribbons of silicene on Ag(110)[21] and 2D monolayers with buckled honeycomb structure on Ag(111)[22, 23] and Ir(111)[24]. Similarly, successful attempts to grow 2D germanium sheets with a honeycomb structure on a platinum(111) and gold(111) template have been reported very recently[25, 26]. As for binary compounds, to the best of our knowledge, no other 2D monolayers beside boron nitride have been synthesized yet[27], even though almost 2D nanoflakes of SiC with thickness of the order of 1 nm have been obtained by means of solution-based exfoliation of SiC crystals[28]. We hope that our work can stimulate further experimental work to fill this gap.

METHODS

Our density functional calculations for buckled AB monolayers were carried out using the projector augmented wave (PAW) method implemented in VASP using the PBEsol functional [29–31]. *d*-electrons are included in the valence in the PAW potentials. Test calculations were also performed using the Heyd-Scuseria-Ernzerhof

(HSE) screened hybrid density functional [32]. The atom positions were optimized until the residual forces were smaller than 0.001 eV/Å with the plane-wave cutoff energy of 500 eV and a set of 8×8×1 k-points for the irreducible BZ. Repeated image interactions were made negligible by including a vacuum layer of 26 Å in the simulations. The FE polarization is calculated using the Berry's phase method [33], and SOC is self consistently taken into account.

The first-principle Berry curvature is calculated according to the usual linear response Kubo-like formula

$$\Omega(\mathbf{k}) = \sum_n f_n \Omega_n(\mathbf{k})$$

$$\Omega_n(\mathbf{k}) = -2Im \sum_{m \neq n} \frac{\langle u_{n\mathbf{k}}|v_x|u_{m\mathbf{k}}\rangle\langle u_{m\mathbf{k}}|v_y|u_{n\mathbf{k}}\rangle}{(E_{m\mathbf{k}} - E_{n\mathbf{k}})^2}, \quad (1)$$

where f_n is the Fermi distribution function, $v_{x,y}$ is the velocity operator, and $u_{n\mathbf{k}}$ is the lattice-periodic eigenvector with eigenvalue $E_{n\mathbf{k}}$ of the Fourier transformed Wannier Hamiltonian as calculated by projecting the DFT Hamiltonian onto a Wannier basis [34].

RESULTS

Starting from the buckled compounds listed in ref.15 we have calculated the buckling heights h (Å), band gaps E_g (eV), barrier heights E_a (eV per formula unit) estimated as the energy difference between the FE buckled structure and the paraelectric planar one, FE polarizations P (10^{-12} C/m) and spin-splittings ΔE_{VB} (ΔE_{CB}) (in meV) at the K point for valence (conduction) bands, see Table I. In this work, we follow previous theoretical studies[15] and assume that atoms A and B belong to the ordered bipartite lattice shown in Fig. 1a), *i.e.*, we neglect the role of disorder[35] ; indeed this effect would require a separate analysis, beyond the purpose of the present study. First we note that if A, B atoms belong to the same group (*i.e.*, IV group), the A-B bond is polar due to the electronegativity difference between A and B, since the electronegativity within a given family of elements decreases on going from the top to a lower period. On the other hand, when A, B atoms belongs to III and V group, respectively, the electronegativity difference becomes even more pronounced (the electronegativity increasing from left to right along the period). The trigonal symmetry and the buckled honeycomb structure imply a local uniaxial dipole moment along the 3-fold rotation axis. By analogy with the Ising model for uniaxial ferromagnets, which is well known to display a phase transition even in the two-dimensional lattice[36], a FE phase transition is indeed possible, where the two symmetry-equivalent energy minima with opposite polarity are obtained by reversing the buckling angle. The estimated FE polarizations of the group IV binary AB monolayers are

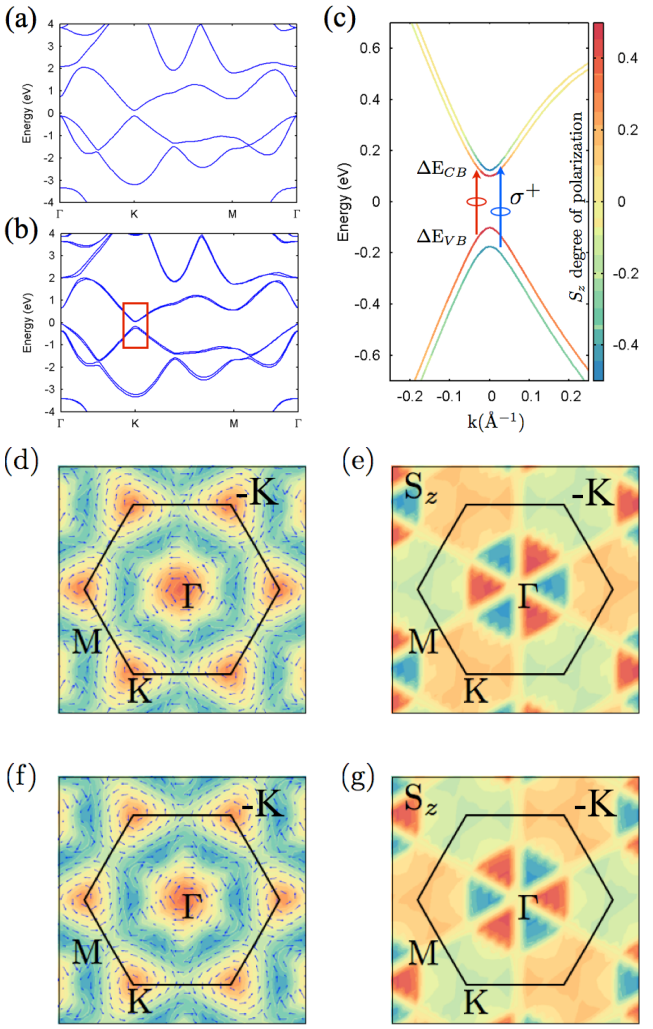

FIG. 2: (a) Band structures along the 2D hexagonal Brillouin zone (BZ) (a) without and (b) with SOC. In (b) the red panel is an eyeguide for the zoomed-in view in (c), where low energy bands around the Fermi level in the vicinity of K are reported. Color scale refers to the out-of-plane S_z spin polarization, while the red and blue arrows, referring to positive and negative S_z spin-component gaps respectively, denote the valley and spin optical transition selection rules for circularly polarized light needed at K for optical interband excitations. (d,e) In-plane and out-of-plane spin textures of the upper and (f,g) lower spin-split VBs for the whole BZ. In (d,f) the color coding refers to the wavevector-dependent energy highlighting the C_{3v} symmetry, while the color scale for the S_z degree of polarization in (e,g) is consistent with (c).

significantly large, with calculated typical values of the order of 1-4 $\times 10^{-12}$ C/m while the group III-V binary AB monolayers have a larger FE polarization, because of the larger electronegativity difference and larger dipole moment carried by each A-B bond. Typical values in this case are around 10 $\times 10^{-12}$ C/m. It is interesting to note that the calculated values for the estimated FE polarizations are always one order of magnitude larger than those

measured in 2D freely-suspended FE smectic-C films[37] and nematic monolayers[38], showing $P \sim 10^{-13}$ C/m. Evaluation of Born effective charges Z^* confirms the estimated values of FE polarization, at the same time providing an estimate of the depolarization field, which is expected to significantly affect the FE properties of thin films. In fact, the electrostatic energy of the depolarization field is proportional to the the square of Z^* and inversely proportional to the electronic polarizability of the material; since the latter is almost constant for all the considered systems, *i.e.* $\varepsilon^{\infty}_{zz} \sim 1$, while Z^* is significantly small (for the zz component of the charge tensor we calculate $Z^*_{zz} \sim 0.05e$ for group IV and $\sim 0.1e$ for group III-V binary AB monolayers), the depolarization field can be expected to be weaker than that preventing ferroelectricity in ultrathin films of ferroelectric perovskites, supporting the feasibility of stable FE distortions. Eventually, the energy barriers E_a calculated for the AB→BA conversion are comparable with those estimated for conventional FE oxides, such as $PbTiO_3$ for which $E_a \sim 0.1 - 0.2$ eV/formula unit, as well as with that of the recently predicted $1T$ FE phase of MoS_2 [39], suggesting that the polarization reversal could be experimentally accessible. Inelastic electron excitations from a STM tip could be also used to switch between the two FE phases, as recently proposed for bistable molecular switches[40, 41].

We discuss then the electronic band structures of a representative example, GeSn, calculated without and with SOC and shown in Fig. 2 (a-b). Band structures for all the other compounds are displayed in the Supplementary Material. The band gap opens at the K point, where both the valence (VB) and conduction (CB) bands are split by SOC, as highlighted in Fig. 2(c). It is also clear from Fig. 2(c) that electrons around the K valley feel a strong Zeeman-like magnetic field, which is responsible for a valley-dependent out-of-plane spin polarization both in the VB and in the CB [9]. The same holds for the -K valley. Due to the time-reversal symmetry, the system remains overall non-magnetic, with opposite out-of-plane spin polarization at time-reversed K and -K points, as clearly shown in Fig. 2 (e),(g). Therefore, the considered buckled FE monolayers show coupled spin and valley physics, thus possibly allowing the spin and valley control similar to layered transition metal dichalcogenides. As for MoS_2 and other group-VI dichalcogenides, the valley Hall effect should be accompanied by a spin Hall effect for both the electron and hole-doped systems, whose robustness can be deduced by the expected long relaxation time of spin and valley indices[13]. Because of the spin-valley coupling and the valley-contrasting spin splittings ΔE_{VB} and Δ_{CB}, the energy conservation would imply a simultaneous flipping of spin and valley indices; since two adjacent valleys are separated by a wave vector comparable with the size of the Brillouin zone, such simultaneous flipping would require atomic scale (magnetic) scatterers. In the absence of such scatterers, both holes and electrons are expected to display long spin and valley lifetimes, therefore allowing robust Hall effects around both the valence and conduction-band edges [13]. The spin textures of the two spin-split VBs calculated for the whole BZ are presented in Fig. 2 (d-g). The typical Rashba spin patterns are clearly observed around K and -K valleys, with the in-plane spin components rotating clockwise or counterclockwise in spin-split bands, as shown in Fig. 2 (d),(f) for upper and lower VBs. Interestingly, while the out-of-plane spin components show opposite polarizations at time-reversed valleys, the in-plane spin components display the same chirality at K and -K points in a single VB; both the Rashba-like chirality and the valley-dependent magnetic moments appear then to be reversed in the other spin-split VB. A similar behaviour is found in the spin-split CBs, while the VB maximum (VBM) and CB minimum (CBM) show same chiralities and out-of-plane polarization direction. When the FE polarization is switched by reversing the buckling, the in-plane spin-texture chiralities are fully reversed, suggesting the possibilities to control the Rashba effect by exploiting the FE properties of binary monolayers. On the other hand, the out-of-plane spin polarization remains exactly the same in opposite FE states. Interestingly, the valley-dependent spin polarization survives even when the buckling is completely suppressed as in the flat graphene-like structure, as a consequence of the non-centrosymmetric, albeit nonpolar, character of the planar honeycomb structure with binary composition.

To understand the origin of this exotic spin and valley physics, and its interplay with the intrinsic FE polarization in buckled trigonal monolayers, we now investigate the microscopic mechanisms underlying the low-energy properties around the Fermi level at the K and -K valleys. In the absence of buckling ($\theta = \pi/2$) and SOC, the low-energy effective Hamiltonian around the K point describing low-energy states with mainly p_z character reads

$$H^{(0)}_{\mathrm{K}} = -m\zeta_z + v_F(\tau k_x \zeta_x - k_y \zeta_y) \qquad (2)$$

where $\boldsymbol{\zeta}$ is the sublattice pseudospin trasforming like Pauli matrices, $\tau = \pm 1$ is a valley index for $\pm K$ points, v_F is the Fermi velocity, and the first "mass" term originates from the different ions located in A and B sublattices. Contrary to the case of graphene, silicene and other group-IV binary monolayers [3, 42–44], the additional mass term leads to an intrinsic gap in the energy spectrum, which opens at the Dirac point (the effective parameters are estimated in a tight-binding framework and given in the Supplementary Material). The VBs and CBs remain spin-degenerate, as sketched in Fig. 3(a) for VBs. When SOC is turned on in the planar structure ($\theta = \pi/2$), additional terms appear in the effective Hamiltonian (2), namely

$$H^{(1)}_{\mathrm{K}} = H^{(0)}_{\mathrm{K}} - \tau\sigma_z\lambda^{+}_{so}\zeta_z - \tau\sigma_z\lambda^{-}_{so} \qquad (3)$$

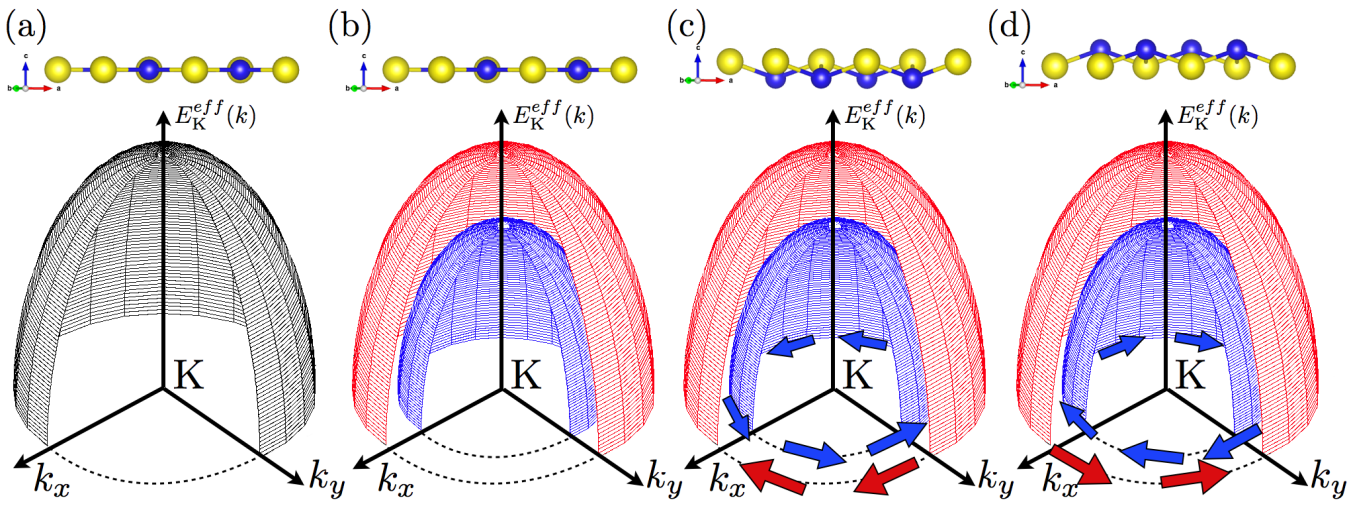

FIG. 3: (a-b) Valence bands (VBs) at the valley without (a) and with (b) SOC in planar AB monolayers. Red and blue colored bands in (b - d) refer to the presence of positive and negative out-of-plane spin polarizations, respectively. (c-d) VBs and relative in-plane spin-texture for positive and negative buckling. Red and blue colored bands still refer to out-of-plane spin polarization, while the arrows are the spin projection on the k_x, k_y plane.

where $\lambda_{so}^{\pm} = (\lambda_{so}^{A} \pm \lambda_{so}^{B})/2$ are effective material-dependent parameters arising from the interplay of atomic SOC constants $\xi_{A/B}$, local orbital energies $\Delta_{A/B}$ and hopping integrals $V_{sp\sigma}$,$V_{pp\sigma}$ and $V_{pp\pi}$, which in turn depend on geometrical factors such as the buckling angle θ (see Supplementary Material). The presence of SOC, therefore, introduces an effective Zeeman-like valley-dependent magnetic field $B^{eff} = -\tau\lambda_{so}^{-}$, which removes the spin-degeneracy without mixing spin up and spin down states, leading to spin-split VBs and CBs with energies $E_\sigma = -\sigma\,\tau\lambda_{so}^{-} \pm \sqrt{(m + \sigma\tau\lambda_{so}^{+})^2 + v_F^2 k^2}$ and a net out-of-plane spin polarizations at the K valleys, as sketched in Fig. 3(b). The VB and CB spin-splittings are listed in Fig. I for all considered binary monolayers, and shown in Fig. 2(c) for the representative case of GeSn. Additionally, the mass term acquires a spin-valley-sublattice contribution $\tau\sigma_z\zeta_z\lambda_{so}^{+}$ which indeed guarantees the coupling between the spin and valley physics. Interestingly, the additional coupling terms experienced by a given sublattice originate from the atomic SOC of the other sublattice mediated by the hopping interactions — in fact, carriers in the A sublattice feel the atomic SOC of B ions through the term $\lambda_{so}^{B}\sigma_z$, and vice versa. This is reflected in the different size of spin-splitting gaps in VBs and CBS. As shown in Fig. 2(c) for the representative case of GeSn, the spin-splitting is larger at VBs rather than at CBs, despite the fact that VBs and CBs show predominant Ge and Sn characters, respectively, as a consequence of the larger electronegativity of Ge. Naïvely, one would expect a larger spin-splitting at CBs than at VBs, since the atomic SOC constant of Sn is larger than that of Ge, $\xi_{Sn} > \xi_{Ge}$.[45] Indeed, the opposite is observed, since carriers with a predominant Ge character experience the SOC-induced interaction coming from the Sn ions, and vice versa. The same holds for all other compounds, as can be inferred looking at values reported in Table 1. It is important to stress that such spin-splitting effects arise uniquely from the binary composition of the monolayers, implying $\lambda_{so}^{-} \neq 0$. The spin-valley coupling, emerging already in the planar noncentrosymmetric binary monolayer, is therefore independent of the buckling distortion; in fact, the $\lambda_{so}^{A/B}$ are even functions of the buckling angle θ, implying that valley-constrating properties such as the out-of-plane spin polarization are not expected to qualitatively change under FE distortions. Furthermore, since the valley-dependent coupling terms do not mix the spin-up and spin-down components, σ_z remains a good quantum number, analogously to what happens in MoS_2 monolayers.

One can easily evaluate the Berry curvature of the Bloch electrons, associated with the valley and spin Hall effect:

$$\Omega_\sigma = \mp\tau \frac{2v_F^2(m + \sigma\tau\lambda_{so}^{+})}{\left[v_F^2 k^2 + (m + \sigma\tau\lambda_{so}^{+})^2\right]^{3/2}}, \tag{4}$$

where the $\mp$ sign refers to CB and VB, respectively, as well as the coupling strength with optical fields of $\hat{\sigma}^{\pm}$ circular polarization:

$$|\mathcal{P}_{\pm}(k)|^2 \propto \left(1 \pm \tau \frac{m + \sigma\tau\lambda_{so}^{+}}{\sqrt{v_F^2 k^2 + (m + \sigma\tau\lambda_{so}^{+})^2}}\right), \tag{5}$$

which display the same form found for MoS_2 monolayers, leading to similar expectations about the robustness of (valley and spin) Hall physics and optoelectronic

effects[13]. In particular, the Berry curvature shows opposite sign in different valleys, while the interband optical transitions are found to be uniquely coupled with $\hat{\sigma}^+$ ($\hat{\sigma}^-$) circularly polarized optical field at the K (-K) valley, the valley optical selection rules being also spin-dependent as shown in Fig. 2 (c). It is also clear from Eqs. (4), (5) that the strength of such spin-valley physics is mainly governed by the spin-valley-sublattice coupling parametrized by λ_{so}^{+}, even though the valley-contrasting spin splitting of both VBs and CBs is due to the effective magnetic field $\tau\lambda_{so}^{-}$.

When ferroelectricity sets in, lowering the trigonal symmetry from C_{3h} to C_{3v} and leading to a finite buckling $\theta \neq \pi/2$, an intrinsic Rashba term must be added in the effective Hamiltonian Eq. (3), namely:

$$H_{\mathrm{K}}^{(2)} = H_{\mathrm{K}}^{(1)} - (\lambda_R^{+}\zeta_z + \lambda_R^{-})(k_y\sigma_x - k_x\sigma_y) \qquad (6)$$

where $\lambda_R^{\pm} = (\lambda_R^A \pm \lambda_R^B)/2$ and $\lambda_R^{A/B}$ is a complex material-dependent parameter which is odd under the switching of the buckling angle (see Supplementary Material). This Rashba coupling term gives rise to in-plane circularly rotating spin-texture around each K valley, with opposite chiralities at spin-split VBs (CBs) as shown in Fig. 3(c)), while substantially not affecting the out-of-plane spin polarization. Neglecting λ_R^{-} for the sake of simplicity, the expectation value for in-plane spin polarizations reads $\langle\sigma_x\rangle \propto -\lambda_R^{+}k_y$ and $\langle\sigma_y\rangle \propto \lambda_R^{+}k_x$ for the VBM and CBM (the overall chirality being fully reversed in the VBM-1 and CBM+1 branches), i.e., the typical Rashba-like behaviour, which appears to be valley-independent, in agreement with our DFT calculations. Since $\lambda_R^{A/B}$ is an odd function of the buckling angle with respect to planar structure $\theta = \pi/2$, the buckling reversal, i.e., the switching of the ferroelectric polarization, leads to a complete reversal of the in-plane Rashba spin-texture chirality only, while the VBs and CBs preserve their out-of-plane spin-polarization, as schematically shown in Fig. 3(c-d). This behaviour perfectly agrees with our first-principles calculations, since its origin lies in the opposite θ-dependence of spin-valley ($\lambda_{so}^{A/B}$) and intrinsic Rashba ($\lambda_R^{A/B}$) coupling constants at, and around, the K point (note that $\lambda_R^{A/B} \neq 0$ only when $\theta \neq \pi/2$ and the k-vector differs from K [43]). It is worthwhile to notice that, although the Rashba-like coupling term causes a mixing of spin-up and spin-down states, the valley physics appears to be robust to buckling distortion. In fact, the Berry curvature has been evaluated from first-principles for the representative GeSn with buckled honeycomb structure, and it has been found to display opposite sign at K and -K valleys, as shown in Fig. 4.

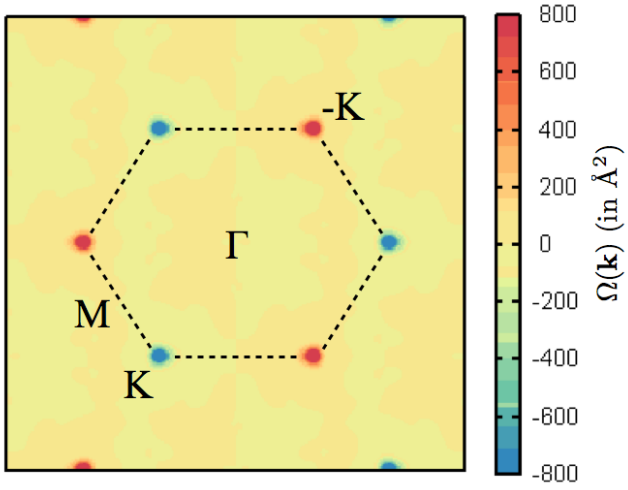

FIG. 4: Momentum resolved first-principles Berry curvature (in Å^2) calculated for GeSn monolayer as a representative example.

CONCLUSIONS

Our first-principles calculations predict a spontaneous FE polarization in buckled group IV and group III-V binary monolayers with trigonal symmetry. Unlike the case of graphene, silicene, germanene and other single atomic type monolayers, the presence of a diatomic basis that breaks the inversion symmetry — even in the planar geometry — leads to the emergence of Zeeman-like spin-split bands with coupled spin-valley physics analogous to the MoS_2 case. At the same time, it is mainly responsible for the onset of the FE phase when the honeycomb lattice buckles, allowing for an electrically controllable Rashba-like spin-texture around the K valleys, whose chirality is locked to the polarization direction and therefore fully reversible upon FE switching. Such Rashba split bands can be effectively detected by spin-resolved spectroscopic techniques, and the process of hole and electron injection allows for the engineering of two dimensional spin field-effect-transistors (FETs) [18]. Even though the spin-valley and Rashba phenomenologies appear to be substantially decoupled, our work suggests a route towards the integration of valleytronic and spintronic features in FE multivalley materials, opening unforeseen possibility in the exciting world of spintronics. Currently the growth of these 2D monolayers on a suitable substrate is difficult, and the effect of the substrate has been only recently addressed [46]. Nevertheless, it is highly desirable to find ways of preparing these fascinating 2D monolayers.

ACKNOWLEDGMENTS

Figures are plotted using VESTA and Gnuplot packages. The authors are thankful to the HPC Center of NCSU for computing resources. A.S. acknowledges

support from CNR Short Term Mobility program prot. ammcnt-cnr0026336 for the visiting stay at IFW Leibniz Institute, Dresden, Germany where this project was conceived and started.

* Electronic address: domenico.disante@aquila.infn.it

[1] A. Rycerz, J. Tworzydo, and C. W. J. Beenakker, Valley filter and valley valve in graphene, Nat. Phys. **3**, 172 (2007).

[2] D. Xiao, W. Yao, and Q. Niu, Valley-contrasting physics in graphene: Magnetic moment and topological transport, Phys. Rev. Lett. **99**, 236809 (2007).

[3] A. H. Castro Neto, F. Guinea, N. M. R. Peres, K. S. Novoselov, and A. K. Geim, The electronic properties of graphene, Rev. Mod. Phys. **81**, 109 (2009).

[4] M.-K. Lee, N.-Y. Lue, C.-K. Wen, and G. Y. Wu, Valley-based field-effect transistors in graphene, Phys. Rev. B **86**, 165411 (2012).

[5] H. Zeng, J. Dai, W. Yao, D. Xiao, and X. Cui, Valley polarization in MoS_2 monolayers by optical pumping, Nat. Nanotech. **7**, 490 (2012).

[6] K. F. Mak, K. He, J. Shan, and T. F. Heinz, Control of valley polarization in monolayer MoS_2 by optical helicity, Nat. Nanotech. **7**, 494 (2012).

[7] T. Cao, G. Wang, W. Han, H. Ye, C. Zhu, J. Shi, Q. Niu, P. Tan, E. Wang, B. Liu, et al., Valley-selective circular dichroism of monolayer molybdenum disulphide, Nat. Commun. **3**, 887 (2012).

[8] K. Behnia, Condensed-matter physics: Polarized light boosts valleytronics, Nat. Nanotech. **7**, 488 (2012).

[9] H. Yuan, M. S. Bahramy, K. Morimoto, S. Wu, K. Nomura, B.-J. Yang, H. Shimotani, R. Suzuki, M. Toh, C. Kloc, et al., Zeeman-type spin splitting controlled by an electric field, Nat. Phys. **9**, 563 (2013).

[10] C. Mai, A. Barrette, Y. Yu, Y. G. Semenov, K. W. Kim, L. Cao, and K. Gundogdu, Many-body effects in valleytronics: Direct measurement of valley lifetimes in single-layer MoS_2, Nano Letters **14**, 202 (2014).

[11] K. F. Mak, K. L. McGill, J. Park, and P. L. McEuen, The valley hall effect in MoS_2 transistors, Science **344**, 1489 (2014).

[12] X. Xu, W. Yao, D. Xiao, and T. F. Heinz, Spin and pseudospins in layered transition metal dichalcogenides, Nat. Phys. **10**, 343 (2014).

[13] D. Xiao, G.-B. Liu, W. Feng, X. Xu, and W. Yao, Coupled spin and valley physics in monolayers of mos_2 and other group-VI dichalcogenides, Phys. Rev. Lett. **108**, 196802 (2012).

[14] D. Xiao, G.-B. Liu, W. Feng, X. Xu, and W. Yao, Coupled spin and valley physics in monolayers of MoS_2 and other group-VI dichalcogenides, Phys. Rev. Lett. **108**, 196802 (2012).

[15] H. Şahin, S. Cahangirov, M. Topsakal, E. Bekaroglu, E. Akturk, R. T. Senger, and S. Ciraci, Monolayer honeycomb structures of group-IV elements and III-V binary compounds: First-principles calculations, Phys. Rev. B **80**, 155453 (2009).

[16] M. Ezawa, Spin valleytronics in silicene: Quantum spin hall-quantum anomalous hall insulators and single-valley semimetals, Phys. Rev. B **87**, 155415 (2013).

[17] E. I. Rashba, Properties of semiconductors with an extremum loop. 1. cyclotron and combinational resonance in a magnetic field perpendicular to the plane of the loop, Sov. Phys. Solid State **2**, 1109 (1960).

[18] D. Di Sante, P. Barone, R. Bertacco, and S. Picozzi, Electric control of the giant rashba effect in bulk GeTe, Advanced Materials **25**, 509 (2013), ISSN 1521-4095.

[19] S. Z. Butler, S. M. Hollen, L. Cao, Y. Cui, J. A. Gupta, H. R. Gutirrez, T. F. Heinz, S. S. Hong, J. Huang, A. F. Ismach, et al., Progress, challenges, and opportunities in two-dimensional materials beyond graphene, ACS Nano **7**, 2898 (2013).

[20] S. Balendhran, S. Walia, H. Nili, S. Sriram, and M. Bhaskaran, Elemental analogues of graphene: Silicene, germanene, stanene, and phosphorene, Small (2014).

[21] B. Aufray, A. Kara, S. Vizzini, H. Oughaddou, C. Leandri, B. Ealet, and G. Le Lay, Graphene-like silicon nanoribbons on ag(110): A possible formation of silicene, Appl. Phys. Lett. **96**, 183102 (2010).

[22] P. Vogt, P. De Padova, C. Quaresima, J. Avila, E. Frantzeskakis, M. C. Asensio, A. Resta, B. Ealet, and G. L. Lay, Silicene: Compelling experimental evidence for graphenelike two-dimensional silicon, Phys. Rev. Lett. **108**, 155501 (2012).

[23] B. J. Feng, Z. J. Ding, S. Meng, Y. Yao, X. He, P. Cheng, L. Chen, and H. Wu, Evidence of silicene in honeycomb structures of silicon on ag(111), Nano Lett. **12**, 3507 (2012).

[24] L. Meng, Y. Wang, L. Zhang, S. Du, R. Wu, L. Li, Y. Zhang, G. Li, H. Zhou, W. A. Hofer, et al., Buckled silicene formation on ir(111), Nano Letters **13**, 685 (2013).

[25] L. Li, S.-Z. Lu, J. Pan, Z. Qin, Y.-Q. Wang, Y. Wang, G.-Y. Cao, S. Du, and H.-J. Gao, Buckled germanene formation on Pt(111), Advanced Materials **26**, 4820 (2014).

[26] M. E. Dávila, L. Xian, S. Cahangirov, A. Rubio, and G. Le Lay, Germanene: a novel two-dimensional germanium allotrope akin to graphene and silicene, New Journal of Physics **16**, 095002 (2014).

[27] P. Miró, M. Audiffred, and T. Heine, An atlas of two-dimensional materials, Chem. Soc. Rev. **43**, 6537 (2014).

[28] S. S. J. Lin, Previous Article Next Article Table of Contents Light-Emitting Two-Dimensional Ultrathin Silicon Carbide, Phys. Chem. C **116**, 3951 (2012).

[29] P. E. Blöchl, Projector augmented-wave method, Phys. Rev. B **50**, 17953 (1994).

[30] G. Kresse and J. Furthmüller, Efficient iterative schemes for ab initio total-energy calculations using a plane-wave basis set, Phys. Rev. B **54**, 11169 (1996).

[31] J. P. Perdew, K. Burke, and M. Ernzerhof, Generalized gradient approximation made simple, Phys. Rev. Lett. **77**, 3865 (1996).

[32] J. Heyd, G. E. Scuseria, and M. Ernzerhof, Hybrid functionals based on a screened coulomb potential, The Journal of Chemical Physics **118**, 8207 (2003).

[33] R. D. King-Smith and D. Vanderbilt, Theory of polarization of crystalline solids, Phys. Rev. B **47**, 1651 (1993).

[34] A. A. Mostofi, J. R. Yates, Y.-S. Lee, I. Souza, D. Vanderbilt, and N. Marzari, Wannier90: A tool for obtaining maximally-localised wannier functions, Comput. Phys. Commun. **178**, 685 (2008).

[35] D. Di Sante, P. Barone, E. Plekhanov, S. Ciuchi, and S. Picozzi, Robustness against Disorder of Rel-

ativistic Spectral Properties in Chalcogenide Alloys, arxiv:1407.2064, (2014).

[36] L. Onsager, Crystal Statistics. I. A Two-Dimensional Model with an Order-Disorder Transition, Phys. Rev. **65**, 117 (1944).

[37] C. Rosenblatt, R. Pindak, N. Clark, and R. Meyer, Freely suspended ferroelectric liquid-crystal films: Absolute measurements of polarization, elastic constants, and viscosities, Phys. Rev. Lett. **42**, 1220 (1979).

[38] Y. Tabe, T. Yamamoto, I. Nishiyama, M. Yoneya, and H. Yokoyama, Ferroelectric nematic monolayer, Jpn. J. Appl. Phys. **42**, L406 (2003).

[39] S. N. Shirodkar and U. V. Waghmare, Emergence of ferroelectricity at a metal-semiconductor transition in a 1T monolayer of MoS_2, Phys. Rev. Lett. **112**, 157601 (2014).

[40] Q. Fu, Y. Luo, J. Yang, and J. Hou, Understanding the concept of randomness in inelastic electron tunneling excitations, Phys. Chem. Chem. Phys. **12**, 12012 (2010).

[41] N. Pavliček, B. Fleury, M. Neu, J. Niedenführ, C. Herranz-Lancho, M. Ruben, and J. Repp, Atomic force microscopy reveals bistable configurations of dibenzo[a,h]thianthrene and their interconversion pathway, Phys. Rev. Lett. **108**, 086101 (2012).

[42] S. Konschuh, M. Gmitra, and J. Fabian, Tight-binding theory of the spin-orbit coupling in graphene, Phys. Rev. B **82**, 245412 (2010).

[43] C.-C. Liu, H. Jiang, and Y. Yao, Low-energy effective hamiltonian involving spin-orbit coupling in silicene and two-dimensional germanium and tin, Phys. Rev. B **84**, 195430 (2011).

[44] N. D. Drummond, V. Zólyomi, and V. I. Fal'ko, Electrically tunable band gap in silicene, Phys. Rev. B **85**, 075423 (2012).

[45] K. Wittel and R. Manne, Atomic spin-orbit interaction parameters from spectral data for 19 elements, Theoret. Chim. Acta (Berl.) **33**, 347 (1974).

[46] A. K. Singh, H. L. Zhuang, and R. G. Hennig, Ab initio synthesis of single-layer III-V materials, Phys. Rev. B **89**, 245431 (2014).